© creative

Scientific paper

# Metal Based Bioactive Nitrogen and Oxygen Donor Mono and Bis Schiff Bases: Design, Synthesis, Spectral Characterization, Computational Analysis and Antibacterial Screening

Sajjad Hussain Sumrra,<sup>1,\*</sup> Wardha Zafar,<sup>1</sup> Sabaahatul Ain Malik,<sup>1</sup> Khalid Mahmood,<sup>2</sup> Syed Salman Shafqat<sup>3</sup> and Saira Arif<sup>1</sup>

<sup>1</sup> Department of Chemistry, University of Gujrat, Gujrat 50700, Pakistan;

<sup>2</sup> Institute of Chemical Sciences, Bahauddin Zakariya University, Multan, Pakistan;

<sup>3</sup> Department of Chemistry, Division of Science and Technology, University of Education, Lahore, Pakistan

\* Corresponding author: E-mail: sajjadchemist@gmail.com/sajjadchemist@uog.edu.pk

Received: 09-30-2021

#### Abstract

The scientific interest in developing the advanced metal based compounds to inhibit and control bacterial infections is continuously rising. Keeping in view their pharmacological significance, two new bioactive symmetrical phenylenediamine mono- and bis-Schiff bases, 2-{[(4-aminophenyl)imino]methyl}-6-methoxyphenol (L¹) and 2,2'-{benzene-1,2-diylb-is[nitrilomethylylidene]}bis(6-methoxyphenol) (L²) have been synthesized and characterized by using physical techniques, spectral methods, elemental and DFT based computational analysis with B3LYP/6-311++G(d, p) basis set. Furthermore, the synthesized ligands were complexed with VO, Mn, Co, Ni, Cu and Zn ions in ratio [M:L,1:2 and 1:1], respectively. All the complexes exhibited significant antibacterial action against all tested bacterial strains. But overall, the zinc complexes possessed higher antibacterial activity. These results concluded that metal complexes might be promising induction in the upcoming time for medical purposes.

**Keywords:** Symmetrical phenylenediamine mono and bis-Schiff bases; computational study; chelation; bidentate and tetradentate; antibacterial activity.

## 1. Introduction

Schiff base ligands occupy significant importance in coordination chemistry as they have potential to form medicinally important metal complexes. They have attained greater attention in biological and coordination chemistry because of their facile preparation, structural variability and diversity. They are significantly involved in the development of chelates. Particularly, the Schiff bases having – OH, –SH and –NH<sub>2</sub> nucleophilic substituents at *ortho* position to the azomethine group have appropriate structures for coordination with metal ions forming more stable metal chelates. Schiff base ligands with electron donors such as nitrogen and oxygen atoms have been extensively investigated because of their competent therapeutic potentials. They are also significant for their biological action against fungi, bacteria<sup>5</sup> and certain types of tumors.

Nowadays, the design and development of new compounds for dealing with resistant microbes have become an important area of antifungal and antibacterial research, as resistance of pathogenic microbes towards already existing antimicrobial drugs is rapidly becoming a worldwide problem. And the discovery of novel metal based antimicrobial agents is one of the most challenging demands for pharmacologists and chemists today.<sup>7</sup> The work highlights the bioactivity of those compounds of first-row divalent and tetravalent transition metals which are non-toxic, economical as well as readily available for pharmacology. Most of the first-row transition metals are essential for biological processes<sup>8</sup> such as respiration, cell division, photosynthesis and nitrogen fixation.9 Apart from choice of transition metals, it is also important to properly design the ligand framework as it has the ability to modify the systematic/oral bioavailability of metals, secure some selective target enzymes or DNA, protect as well as supply metal ions at targeted sites. <sup>10</sup>

Slight modifications in the structure of ligand could significantly increase the pharmacological properties of metal complexes through the endorsement of bioactive metal ions. The metal complexes of Schiff bases have been known to possess different biological activities like antifungal, anticumer, anticumer

With the expansion of our research work describing the synthesis, structure elucidation and pharmacological properties of chemical scaffolds prepared by the condensation of phenylenediamine with aromatic carbonyls,<sup>27</sup> here we report the facile synthesis of two new phenylenediamine derived mono- and bis-Schiff bases, 2-{[(4-aminophenyl)imino]methyl}-6-methoxyphenol (L¹) and 2,2'-{benzene-1,2-diylbis[nitrilomethylylidene]}bis(6-methoxyphenol) (L<sup>2</sup>) and their complexes with VO(IV), Mn(II), Co(II), Ni(II), Cu(II) and Zn(II) metals. All the synthesized compounds have been studied in detail for their structure, physicochemical and in vitro antibacterial properties against one Gram positive bacteria (GPB) and one Gram negative bacteria (GNB). Density functional parameters have been utilized for analysing the molecular designs, active sites, molecular interactions along with biochemical activity. The experimental findings have been compared to their computed results.

# 2. Experimental

#### 2. 1. Materials

Chemicals of analytical grade were used during the research work. *o*-Phenylenediamine, *p*-phenylenediamine and 2-hydroxy-3-methoxybenzaldehyde were purchased from Sigma Aldrich which were extremely pure so they were used without further purification. Ethanol and dioxane were distilled for the additional refinement because they have been used as solvents in the reaction media for the synthetic reactions of ligands and their corresponding metal chelates, respectively.

#### 2. 2. Instrumentation

The melting temperatures of ligands and decomposition temperatures of metal complexes were determined using Stuart apparatus. FT-IR spectra were documented using Nicolet FT-IR Impact 400D infrared Spectropho-

tometer in working range (4000-400 cm<sup>-1</sup>). Proton NMR spectra of the mono- and bis-Schiff bases were obtained through Bruker Advance 300 MHz using DMSO (dimethyl sulfoxide) solvent. The mass spectra of ligands were taken on JEOL MS Route instrument. UV-Vis spectra were recorded on Hitachi UV-3200 spectrophotometer using DMF (dimethyl formamide) solvent. Magnetic moment values for the metal complexes were recorded with the Magnetic Susceptibility Balance (MSB Mk-1) using MnCl<sub>2</sub> as a reference. Molar conductivity measurements of metal complexes (0.001M solutions in DMF) were carried out using Inolab Cond 720 Conductivity Bridge at room temperature. The antibacterial activity was performed using DMSO solvent on ESCO Laminar Flow Cabinet and Memmert incubator at the Department of Biochemistry, University of Gujrat, Gujrat, Pakistan.

#### 2. 3. Synthesis of Ligands

The phenylenediamine based ligands, 2-{[(4-aminophenyl)imino[methyl]-6-methoxyphenol ( $L^1$ ) and 2,2'-{benzene-1,2-diylbis[nitrilomethylylidene]}bis(6-methoxyphenol) (L<sup>2</sup>) have been synthesized by adopting already published path<sup>28</sup> as shown in Scheme 1. The *p*-phenylenediamine ligand (L1) was synthesized by adding the equimolar amount of ethanolic solution of 2-hydroxy-3-methoxybenzaldehyde (10 mmol, 1.52 g) over a stirred ethanolic solution of p-phenylenediamine (10 mmol, 1.08 g). Change in colour and precipitate formation in the reaction mixture was the first indication of the successful reaction. The reaction mixture was continuously stirred and the advancement in the reaction mixture was checked by taking comparative thin layer chromatography (TLC). The finishing point of the reaction was evidenced through a single spot of ligand on the TLC. The precipitates of ligand were then filtered out, rinsed with warm ethanol, dried off and then recrystallized by 1:2 ratio of ethanol and ether to obtain the pure product. The o-phenylenediamine ligand ( $L^2$ ) was also synthesized by the same pathway through refluxing instead of stirring the ethanolic solution of o-phenyl-

Scheme 1. Synthesis of phenylenediamine Schiff base ligands (L $^1$ ) & (L $^2$ )

enediamine (5 mmol, 0.54 g) with same 2-hydroxy-3-methoxybenzaldehyde (10 mmol, 1.52 g) in 1:2 molar ratio.

# 2. 3. 1. 2-{[(4-Aminophenyl)imino]methyl}-6-methoxyphenol (L¹)

Yield (%): 82; m.p. (°C): 256; colour: light yellow; IR (KBr, cm<sup>-1</sup>): 3427 (OH), 3020 (NH<sub>2</sub>), 2930 (OCH<sub>3</sub>), 1640 (HC=N), 1389 (C-O); <sup>1</sup>HNMR (DMSO- $d_6$ , 300 MHz)  $\delta$  (ppm): 3.82 (s, 3H, OCH<sub>3</sub>), 6.90-7.26 (m, 7H, Ar-H), 7.53 (s, 2H, NH<sub>2</sub>), 9.01 (s, 1H, HC=N), 13.17 (s, 1H, OH); MS (ESI) m/z (%): 241.1 ([M]<sup>+</sup>, 100), 227.1 (24), 209.1 (09), 197.0 (08), 183.0 (05), 154.0 (10), 135.0 (04); Anal. calcd. for C<sub>14</sub>H<sub>14</sub>N<sub>2</sub>O<sub>2</sub> (%) C, 69.4; N, 11.56; H, 5.82; found: C, 69.35; N, 11.49; H, 5.78.

# 2. 3. 2. 2,2'-{Benzene-1,2-diylbis[nitrilomethyly-lidene]}bis(6-methoxyphenol) (L<sup>2</sup>)

Yield (%): 73; m.p. (°C) 173; colour: dark orange; IR (KBr, cm<sup>-1</sup>): 3431 (OH), 3100 (C-H), 2918 (OCH<sub>3</sub>), 1638 (HC=N), 1396 (C-O); <sup>1</sup>HNMR (DMSO- $d_6$ , 300 MHz,)  $\delta$  (ppm): 3.92 (s, 3H, OCH<sub>3</sub>), 6.88-6.93 (t, 1H, C<sub>8</sub>-H, C<sub>18</sub>-H), 6.95-6.97 (d, 1H, C<sub>9</sub>-H, C<sub>19</sub>-H), 7.07-7.13 (dd, 1H, C<sub>7</sub>-H, C<sub>23</sub>-H), 7.23-7.28 (d, 1H, C<sub>3</sub>-H), 7.38-7.46 (m, 1H, C<sub>1</sub>-H, C<sub>2</sub>-H), 7.60-7.64 (d, 1H, C<sub>6</sub>-H), 8.91 (s, 1H, HC=N), 12.97 (s, 1H, OH); MS (ESI) m/z (%): 376.4 ([M]<sup>+</sup>, 100), 361.2 (36), 253.1 (25), 240.1 (62), 222.1 (28), 211.1 (22), 197 (14). Anal. Calcd. for C<sub>22</sub>H<sub>20</sub>N<sub>2</sub>O<sub>4</sub> (%): C, 70.20; N, 7.44; H, 5.36; found: C, 69.96; N, 7.38; H, 5.31.

# 2. 4. Synthesis of Transition Metal Complexes

All the transition metal complexes of p-phenylenediamine ligand ( $L^1$ ) were synthesized using 1:2 molar ratio

of metal to ligand by accomplishing previously reported protocol.<sup>28</sup> The ligand (20 mmol) was dissolved in 10 mL dioxane and magnetically refluxed until the ligand was completely dissolved. Then, the respective metallic salt (vanadyl sulphate hydrate, manganese(II) chloride, cobalt(II) chloride hexahydrate, nickel(II) chloride hexahydrate, copper(II) chloride dihydrate and anhydrous zinc(II) chloride) solution (10 mmol) was gradually added in the ligand solution with continual stirring. After that, the reaction mixture was further refluxed for 6 hours. The reaction was observed by using TLC at regular intervals. Desired products were obtained in the form of the precipitates, which were filtered, washed with hot dioxane, dried and then recrystallized using dioxane and ether (1:2) to obtain the pure product. For the synthesis of metal complexes of o-phenylenediamine ligand ( $L^2$ ), same procedure was fallowed except that ligand (L1) was replaced with ligand (L<sup>2</sup>) and equimolar ratio of ligand and metal salts were used. All complexes were synthesized according to above mentioned procedure and their structures are shown in Scheme 2.

# 2. 5. Computational Study

Both the ligands ( $L^1$ ) and ( $L^2$ ) and their selected 3d-metal complexes have been optimized by density functional theory (DFT) to insight their geometries in absence of their well resolved SC-XRD data. For this computational study, the Gaussian 09 program<sup>29</sup> was employed to execute all the theoretical simulations for molecular dynamics with the help of DFT. Based on the B3LYP method with 6-311++G(d, p) basis sets, the molecular geometries of compounds were thoroughly optimized at their ground state energy levels. The HOMO-LUMO energies together with their energy differences for optimized structures were

Scheme 2. Synthesis of phenylenediamine metal based compounds (1)-(12)

calculated to analyse their quantum chemical parameters. The structural characteristics, stability and molecular quantities i.e., chemical softness, hardness and electronegativity, electrophilicity were determined satisfactorily.<sup>30</sup> The computed FT-IR spectra of the studied molecular systems have also been established from their optimized geometrical structures through B3LYP/6-311++G(d, p) functions. The natural bond orbital (NBO) analysis, Mulliken atomic charges (MAC) and molecular electrostatic potential (MEP) maps of the studied molecules have been assessed at the same functional, whereas UV-Vis spectra have been computed employing the TD-DFT (time-dependent density functional theory) accompanied by the afore-mentioned functional. Furthermore, all the input data files were structured using Gaussview 5.0.31 While GaussSum,<sup>32</sup> Avogadro,<sup>33</sup> Chemcraft<sup>34</sup> and Gaussview 5.0 programs have been utilized to interpret and visualize the outcomes of the optimized structures, computed spectra along with the summary of their geometrical parameters like bond lengths and bond angles.

#### 2. 6. Antibacterial Study

Anti-bacterial action of the prepared compounds was evaluated against three G- bacteria (GNB) *i.e.*, *Salmonella typhi*, *Klebsiella pneumonia*, *Escherichia coli* and one Gram+bacteria (GPB) *i.e.*, *Staphylococcus aureus* through disc dif-

fusion method.<sup>35</sup> Standard drugs ampicillin and streptomycin were used to compare the results. Equivalent quantity of both nutrient broth and agar-agar were mixed up in distilled water. The synthesized media, filter paper strips and petri dishes were autoclaved for about 30 minutes at 121 °C for sterilization. Then, the semi-liquid media was transferred to petri dishes and allowed to solidify. After that, the bacterial inoculum was spread over the media by means of glass spreader. Later on, the filter paper strips were placed at the regular distance on the solidified media. Then, 10 µL of DMSO, sample solutions and standards having same concentration (2 mM in DMSO) were poured onto the strips via micropipette. In this analysis, DMSO and standards acted as negative and positive controls, correspondingly. The plates were properly labelled for each sample and standard, tightly wrapped and placed in incubator at 37 °C temperature for 24 hours. Finally, the inhibition zones of the tested samples and standards were checked and recorded in millimetre (mm) against each bacterial strain.

# 3. Results and Discussion

The symmetrical Schiff base ligands ( $L^1$ ) and ( $L^2$ ) were prepared in 1:1 and 1:2 molar ratio by condensation reaction of o-vanillin with p-phenylenediamine and o-phenylenediamine, respectively. The synthesized ligands

Table 1. Physical, analytical	and elemental	details of metal	complexes (1)-(1	2)
-------------------------------	---------------	------------------	------------------	----

	Compound	Formula	M.W (g/mol)	Calculated (%) (Found)			
No	M.P (°C)	Colour	Yield (%)	C	H	N	M
(1)	$VO(L^1)_2$	C <sub>28</sub> H <sub>26</sub> N <sub>4</sub> O <sub>5</sub> V	547.47	61.20	4.77	10.20	9.27
	300+	Pine green	65	(61.08)	(4.65)	(10.11)	(9.14)
(2)	$Mn(L^{1})_{2}(H_{2}O)_{2}$	$C_{28}H_{30}N_4O_6Mn$	573.50	58.64	5.27	9.77	9.58
	283-285	Dark brown	78	(58.59)	(5.21)	(9.68)	(9.45)
(3)	$Co(L^{1})_{2}(H_{2}O)_{2}$	$C_{28}H_{30}N_4O_6Co$	577.49	58.23	5.24	9.70	10.20
	277–279	Russet Brown	70	(58.18)	(5.19)	(9.64)	(10.07)
(4)	$Ni(L^{1})_{2}(H_{2}O)_{2}$	$C_{28}H_{30}N_4O_6Ni$	577.25	58.26	5.24	9.71	10.17
	289-291	Cyan	72	(58.18)	(5.16)	(9.63)	(10.09)
(5)	$Cu(L^1)_2(H_2O)_2$	$C_{28}H_{30}N_4O_6Cu$	582.11	57.77	5.19	9.62	10.92
	293–295	Olive green	82	(57.65)	(5.08)	(9.53)	(10.88)
(6)	$Zn(L^{1})_{2}(H_{2}O)_{2}$	$C_{28}H_{30}N_4O_6Zn$	583.94	57.59	5.18	9.59	11.20
	264–266	Off-white	72	(57.51)	(5.07)	(9.50)	(11.06)
(7)	$VO(L^2)$	$C_{22}H_{18}N_2O_5V$	441.33	59.87	4.11	6.35	11.54
	265-267	Greenish black	72	(59.73)	(4.05)	(6.31)	(11.47)
(8)	$Mn(L^2)(H_2O)_2$	$C_{22}H_{22}N_2O_6Mn$	465.37	56.78	4.77	6.02	11.81
	276–278	Brownish green	68	(56.64)	(4.72)	(5.96)	(11.76)
(9)	$Co(L^2)(H_2O)_2$	$C_{22}H_{22}N_2O_6Co$	469.35	56.30	4.72	5.97	12.56
	248-250	Dark violet	77	(56.17)	(4.67)	(5.90)	(12.50)
(10)	$Ni(L^2)(H_2O)_2$	$C_{22}H_{22}N_2O_6Ni$	469.1	56.33	4.73	5.97	12.51
	260-262	Dark grey	83	(56.18)	(4.68)	(5.93)	(12.43)
(11)	$Cu(L^2)(H_2O)_2$	$C_{22}H_{22}N_2O_6Cu$	473.97	55.75	4.68	5.91	13.41
•	230–232	Greenish black	82	(55.65)	(4.64)	(5.88)	(13.47)
(12)	$Zn(L^2)(H_2O)_2$	$C_{22}H_{22}N_2O_6Zn$	475.83	55.53	4.66	5.89	13.74
	239–241	Off-white	81	(55.41)	(4.60)	(5.83)	(13.66)

were moisture and air stable. Both the ligands were completely soluble in DMSO, DMF and dioxane at room temperature. Both these ligands were then reacted with metallic salts VOSO<sub>4</sub>·H<sub>2</sub>O, MnCl<sub>2</sub>·2H<sub>2</sub>O, NiCl<sub>2</sub>·6H<sub>2</sub>O, CoCl<sub>2</sub>· 6H<sub>2</sub>O, CuCl<sub>2</sub> · 2H<sub>2</sub>O and ZnCl<sub>2</sub> to synthesize 3d-metal complexes in metal to ligand molar ratio of 1:2 and 1:1, respectively (Scheme 1). All the as-synthesized metal chelates were microcrystalline solids having intense colours except zinc complexes which were colourless. The metal complexes exhibited greater range of decomposition points with regard to their respective ligands as a result of strong bonding in metal chelates. The structures of synthesized phenylenediamine Schiff bases and their corresponding 3d-metal chelates were explored on the basis of their spectral, physical and micro-analytical results. The non-electrolytic behaviour of the metal chelates was specified by their minor conductance values. The spectral results together with elemental analysis agreed well with the proposed structures of the as-synthesized compounds, verifying their high purity (given in Table 1).

#### 3. 1. FT-IR Spectra

The IR spectra of both ligands showed a typical peak of azomethine linkage (HC=N) at 1638-1640 cm<sup>-1</sup> that gave a clue about the condensation of amine (-NH<sub>2</sub>) group of phenylenediamine with carbonyl (C=O) group of 2-hydroxy-3-methoxybenzaldehyde. Moreover, the ligands also exhibited different bands at 3427-3431, 2918-2930 and 1389–1396 cm<sup>-1</sup> because of the existence of  $\nu(OH)$ ,  $\nu(OCH_3)$  and  $\nu(C-O)$  groups, respectively.<sup>36</sup> The vibrational spectrum of ligand (L1) demonstrated a peak at 3020 cm<sup>-1</sup> (Figure S1) signifying the non-participation of one amino (NH<sub>2</sub>) group of p-phenylenediamine moiety in the condensation process, consequently validating the synthesis of mono-Schiff base (L1). While the characteristic peaks of both amino (NH<sub>2</sub>) groups of o-phenylenediamine moiety were missing in the spectrum of ligand (L<sup>2</sup>) confirming the synthesis of bis-Schiff base (Figure S2).

IR spectra of the phenylenediamine Schiff bases (L1) and (L2) have been compared with metal complexes and showed that the Schiff bases were bonded with metal ions in bidentate and tetradentate mode, respectively (Table 2). Coordination of both ligands with 3d-metallic ions occurred via oxygen atom of benzaldehyde by the deprotonation of phenolic group and nitrogen atom of azomethine (Figure S3-S4). The coordinating action of the azomethine-N with the metal atoms was confirmed from the shifting of the IR band of azomethine (CH=N) linkage from 1638-1640 cm<sup>-1</sup> to lower frequency at 1620-1630 cm<sup>-1</sup>.<sup>37</sup> The absence of band at 3427–3431 cm<sup>-1</sup> because of  $\nu$ (OH) group accompanied by the shifting of  $\nu$ (C–O) band from 1389-1396 cm<sup>-1</sup> to 1381-1388 cm<sup>-1</sup> indicated the deprotonation of phenolic group of the ligands and its coordination with metal ions.<sup>38</sup>

Existence of new weak bands at 431–440 and 523–539 cm<sup>-1</sup> in the metal complexes, were allocated to v(M-O) and v(M-N) vibrations, correspondingly<sup>39</sup> and these vibrational bands were not observed in the spectra of the uncomplexed ligands. A peak was emerged at 968–972 cm<sup>-1</sup> only in the vibrational spectra of VO(IV) complexes (1) and (7) which was owing to v(V=O). New broad peaks appearing in all the complexes except vanadium complexes at 3423–3479 cm<sup>-1</sup> were due to existence of H<sub>2</sub>O molecules. There was no change in IR bands of methoxy (OCH<sub>3</sub>) group indicating that it was not involved in the complexation. All these evidences confirmed that the ligands bonded with the respective metal cations by azomethine-N along with benzaldehydic-O by the deprotonation of phenolic group.

## 3. 2. UV-Vis Spectra

The experimental UV-Vis spectra of all the as-synthesized complexes were recorded in dimethylformamide using  $10^{-1}\,\mathrm{M}$  concentration. The UV–Vis spectra of ligands have shown a band at 282–297 nm attributed to  $\pi$ – $\pi$ \* electronic structure of aromatic ring system. However, the

Table 2. Magnetic,	conductivity and	ik spectrai data o	i metai compiexes	(1)– $(12)$

No.	μ <sub>eff</sub> (B.M)	$\Omega_{M} \ (\Omega^{-1} { m cm}^{2} { m mol}^{-1})$	ν (cm <sup>-1</sup> )
(1)	1.72	13.5	3153 (NH <sub>2</sub> ), 1625 (C=N), 972 (V=O), 538 (V-N), 434 (V-O)
(2)	5.78	12.9	3479 (H <sub>2</sub> O), 3128 (NH <sub>2</sub> ), 1622 (C=N), 535 (Mn-N), 432 (Mn-O)
(3)	4.34	15.4	3477 (H <sub>2</sub> O), 3140 (NH <sub>2</sub> ), 1626 (C=N), 547 (Co-N), 445 (Co-O)
(4)	3.07	17.6	3467 (H <sub>2</sub> O), 3152 (NH <sub>2</sub> ), 1620 (C=N), 528 (Ni-N), 440 (Ni-O)
(5)	1.81	19.2	3423 (H <sub>2</sub> O), 3167 (NH <sub>2</sub> ), 1621 (C=N), 540 (Cu-N), 439 (Cu-O)
(6)	Dia	15.6	3470 (H <sub>2</sub> O), 3145 (NH <sub>2</sub> ), 1627 (C=N), 549 (Zn-N), 435 (Zn-O)
(7)	1.76	12.7	1622 (C=N), 972 (V=O), 528 (V-N), 439 (M-O)
(8)	5.85	17.2	3429 (H <sub>2</sub> O), 1620 (C=N), 535 (Mn-N), 431 (Mn-O)
(9)	4.21	14.8	3475 (H <sub>2</sub> O), 1628 (C=N), 537 (Co-N), 437 (Co-O)
(10)	3.11	22.3	3445 (H <sub>2</sub> O), 1625 (C=N), 528 (Ni-N), 440 (Ni-O)
(11)	1.87	15.4	3470 (H <sub>2</sub> O), 1623 (C=N), 539 (Cu-N), 437 (Cu-O)
(12)	Dia	18.3	3473 (H <sub>2</sub> O), 1630 (C=N), 530 (Zn-N), 433 (Zn-O)

other absorption bands were documented as  $\lambda_{max}$  at the 339–364 and 395–407 nm owing to  $n-\pi^*$  electronic transitions by the azomethine linkage together with charge transfer, correspondingly.<sup>42</sup> The vanadium(IV) complexes, (1) and (7) exhibited their characteristic bands in the range of 374–387, 529–536 and 733–747 nm as a result of the electronic transitions that were referred to  $B_2 \rightarrow E_{\pi}$ ,  $B_2 \rightarrow B_1$  and  $B_2 \rightarrow A_1$  thus validating their predicted square pyramidal geometry.<sup>43</sup> The three bands in the UV-Vis spectra of manganese(II) complexes (2) and (8) were observed at 221–233 nm 251–267 nm and 342–356 nm due to intra-ligand electronic transitions and  $^6A_{1g} \rightarrow ^4E_g$  therefore verifying their proposed octahedral geometry.

The cobalt(II) complexes (3) and (9) had shown a high energy band of 327-348 nm along with the low energy absorption bands ranging from 506-586 and 1135-1157 nm because of  ${}^{4}T_{1g}(F) \rightarrow {}^{4}T_{1g}(P)$  and  ${}^{4}T_{1g}(F) \rightarrow {}^{4}T_{2g}(F)$  electronic transitions evidencing their anticipated octahedral geometrical structure.44 The three electronic bands of nickel(II) complexes (4) and (10) were observed in the range of 389-425, 617-645 and 1024-994 nm owing to  ${}^{3}T_{2g}(F) \rightarrow {}^{3}T_{1g}(P), {}^{3}A_{2g}(F) \rightarrow {}^{3}T_{1g}(F) \text{ and } {}^{3}A_{2g}(F) \rightarrow {}^{3}T_{2g}(F)$ electronic transitions proving their estimated octahedral geometry. The copper(II) complexes, (5) and (11) demonstrated two absorption bands at 518-524 and 631-674 nm due to  ${}^2B_{1g}{
ightarrow}{}^2E_g$  and  ${}^2B_{1g}{
ightarrow}{}^2A_{1g}$  excitations as well as a highly intense band as a result of metal-ligand charge transfer (MLCT) at 338-345 nm suggesting their octahedral geometry. 45 Only a strong band owed to MLCT at 322-336 nm was recorded for zinc(II) complexes (6) and (12), signifying the absence of d-d transitions and confirming their anticipated octahedral geometry.<sup>46</sup>

# 3. 3. <sup>1</sup>H-NMR Spectra

<sup>1</sup>HNMR spectra of the phenylenediamine Schiff bases (L<sup>1</sup>) and (L<sup>2</sup>) were determined in DMSO- $d_6$ . All the aromatic as well as heteroaromatic protons were observed in their estimated ranges. In the spectra of both ligands, the distinctive singlet peak of imine (HC=N) proton was spotted at 8.91-9.01 ppm. While in the spectrum of ligand (L<sup>1</sup>), the singlet peak of two amino (NH<sub>2</sub>) protons was observed at 7.53 ppm, signifying that only one amino group of p-phenylenediamine was condensed with o-vanillin, indicating the synthesis of mono-Schiff base ligand (Figure S5). While the absence of both amino (NH<sub>2</sub>) group of o-phenylenediamine (Figure S6) specified the synthesis of bis-Schiff base ligand ( $L^2$ ). The peaks of methoxy (OCH<sub>3</sub>) group protons of both Schiff bases were observed as singlet at 3.82-3.92 ppm. The aromatic protons were appeared in the range 6.88–7.64 ppm. Furthermore, the phenolic (OH) group protons were found at 12.97-13.17 ppm as singlet. Absence of aldehydic (CH=O) group protons in the spectra of both ligands, confirmed that the condensation phenomenon was occurred between phenylenediamine and o-vanillin.

#### 3. 4. Mass Spectra

The mass spectra of both phenylenediamine Schiff bases showed the molecular weights (m/z) and base peaks (%). The base peak as well as molecular ion peak of the ligand ( $\mathbf{L^1}$ ) was found at m/z 241.1 due to  $[C_{14}H_{13}N_2O_2]^+$  fragment (Figure S7). While the ligand ( $\mathbf{L^2}$ ) displayed molecular ion peak of  $C_{22}H_{20}N_2O_4$  fragment at m/z 376.4 that was equivalent to its molecular weight (Figure S8). This was also the most stable fragment. Similarly, all the daughter fragments were obtained by the cleaving action of exocyclic as well as endocyclic (C=N) and (C=C) groups. The results of mass spectra evidently confirmed the synthesis of both phenylenediamine Schiff bases with their proposed structures.

# 3. 5. Molar Conductivity and Magnetic Moment Measurements

The molar conductivity measurements of the synthesized metal complexes have been carried out at room temperature using dimethylformamide solvent and the conductivity readings are depicted in Table 2. The complexes were found to be non-electrolytes in nature as their molar conductance values were observed in the range 12.7–22.3  $\Omega^{-1} \text{cm}^2 \text{mol}^{-1}$ . The findings of molar conductivity analysis declared all the metal complexes as neutral having no free anions outside the coordination sphere.

Magnetic moments have contributed valuable details regarding the number of unpaired electrons together with stereochemistry of metal cations, leading towards the determination of the appropriate geometries of the complexes. Depending on the magnetic influence of the unpaired electrons, some metal complexes have shown greater values of magnetic moments while others presented lesser magnetic moments (as given in Table 2). The vanadyl complexes (1) and (7) had the magnetic moment values of 1.72-1.76 B.M which showed one unpaired electron and thus confirmed a square pyramidal configuration for both VO(IV) complexes.<sup>48</sup> The Mn(II) complexes (2) and (8) have exhibited 5.78-5.85 B.M that pointed towards the presence of five unpaired electrons suggesting octahedral arrangement.<sup>49</sup> The Co(II) complexes (3) and (9) displayed the magnetic moments at 4.21-4.34 B.M, signifying complexes have high spins with three unpaired electrons present in an octahedral geometry.<sup>50</sup> The measured magnetic moments of nickel complexes (4) and (10) were found at 3.07-3.11 B.M representing the existence of two unpaired electrons thus signifying an octahedral configuration for Ni(II) complexes.<sup>51</sup> The magnetic moments for Cu(II) complexes (5) and (11) have been observed as 1.81-1.87 B.M representing only one unpaired electron for each copper metal ion with d<sup>9</sup>-system indicating octahedral geometry for copper complexes.<sup>52</sup> The Zn(II) complexes (6) and (12) had zero magnetic moment showing no unpaired electron thus both the complexes were found to be diamagnetic in nature as expected.<sup>53</sup>

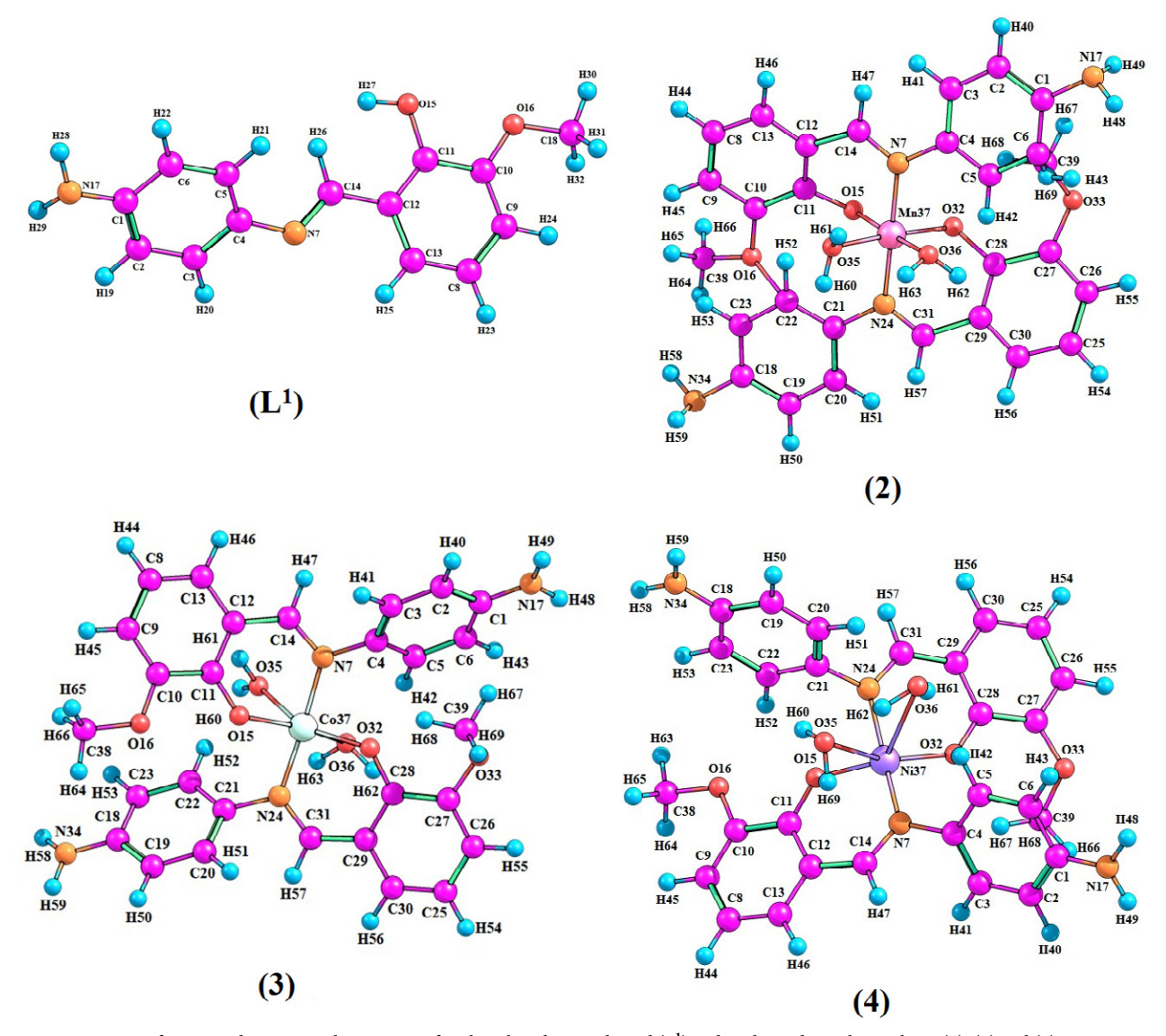


Figure 1. View of optimized geometrical structures of p-phenylenediamine ligand ( $L^1$ ) and its derived metal complexes (2), (3) and (4)

## 3. 6. Molecular Geometric Parameters

Complete process of geometry optimization has been accomplished without any symmetry restriction by employing B3LYP level of DFT in combination with basis set 6-311++G(d, p). The vibrational analysis employing DFT/B3LYP/6-311++G(d, p) level of theory has also been carried out to further validate the stability related with optimized geometrical structures. No hypothetical frequency was detected from the vibrational scrutiny of investigated compounds, which signified the completion of their geometry optimization. Figures 1 & 2 illustrate the molecular structure of all the studied compounds with atom numbering. The optimized geometrical elements including bond angles together with bond lengths were estimated with DFT study by the B3LYP level, and the representative outcomes are given in Table S1 (Supplementary Information).

For complexes (2), (3) and (4), the bond lengths of C4-N7, N7-C14 and C11-O15 were increased, because of the reason that the chelation occurred *via* N7, O15 with metallic centres (Mn, Co and Ni). Similarly for complexes (7), (11) and (12), increase in C5-N13, N13-C15, C4-N14, N14-O24, O16-C11 and O25-C21 bond lengths was observed as a result of the complexation *via* N13, N14, O16, O25 with metallic centres (V, Cu and Zn). This increase in bond lengths signified that the ligands (L¹) and (L²) coordinated *via* N7, O15 and N13, N14, O16, O25 with divalent and tetravalent metallic centres, respectively. The formations of the M-N and M-O bonds resulted in the weakness of C-N and C-O bonds, correspondingly.

All the bond lengths of ligands  $(L^1)$  and  $(L^2)$ , which were involved in coordination have shown an increase in the lengths signifying the establishment of M–N and M–O bonds in all the studied metal complexes. Moreover, the

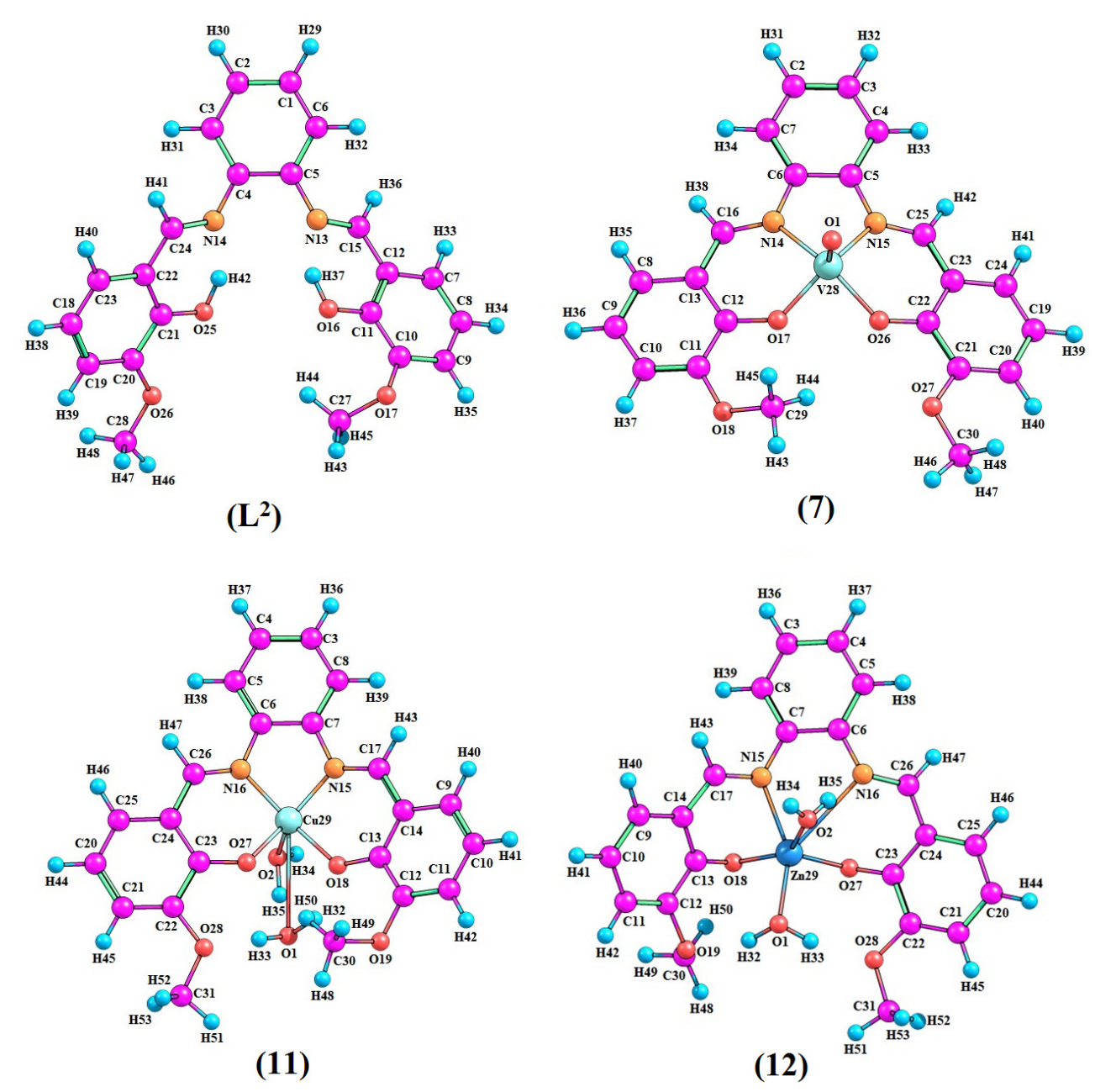


Figure 2. View of optimized geometrical structures of o-phenylenediamine ligand (L2) and its derived metal complexes (7), (11) and (12)

other bond lengths of the ligands were also significantly influenced by the coordination. Bond lengths of M–N bonds were greater than that of M–O bonds that gave the indication for stronger coordination of metal centers with oxygen atom of benzaldehyde by the deprotonation of phenolic group rather than nitrogen atom of azomethine linkage.

# 3. 7. Frontier Molecular Orbitals (FMOs) Analysis

The highest occupied molecular orbital (HOMO) designates the electron donation while the lowest unoc-

cupied molecular orbital (LUMO) designates electron acceptance aptitude. The electronic transitions produced in consequence of the dipole moments arising amongst the ground and excited states of studied chemical entities are responsible for the optical features, electrical attributes and molecular chemical stability together with reactivity. In most of the cases, a transitions occur from HOMO to LUMO. Furthermore, the energy gap ( $\Delta E$ ) between these molecular orbitals is the main parameter to assign and explain reactivity and stability of the studied compounds.  $^{54}$ 

For newly synthesized phenylenediamine ligands  $(L^1)$ – $(L^2)$  and their selective metal complexes, the energies

of molecular orbitals including LUMO and HOMO, along with their energy differences have been computed by employing B3LYP/6-311++G(d, p) basis sets (as shown in Table 3). While the FMO's interpreting the distribution of electron charge density are illustrated in Figure 3. The DFT obtained results have shown that ligands  $(L^1)$  and  $(L^2)$  exhibited 491 and 749 molecular orbitals, respectively. From these orbitals, 64-65 and 99-100 were established as HO-MO-LUMO for both ligands, correspondingly. It is evaluated that the FMO energy gap calculated for HOMO→LU-MO in ligand  $(L^1)$  was more than that in ligand  $(L^2)$ . The FMO energy gap HOMO $\rightarrow$ LUMO was 3.693 eV for (L<sup>1</sup>), which decreased to 3.653 eV in (L2). This reduction in the band difference for  $(L^2)$  may be because of the presence of noncovalent attraction as well as extended conjugation in contrast to  $(L^1)$ .

In both studied structures of the ligands, an evident intramolecular transfer of charge occur from the middle part (HOMO) to the ultimate part (LUMO), therefore giving appropriate explanations to use these studied ligands in phenomenon of charge transfer. Overall, the acquired details signified that the ligand ( $L^2$ ) has shown small energy difference contrary to other ligand ( $L^1$ ), which describes

greater intra-molecular charge transfer (ICT) communication within the ligand (L²). The trend for  $\Delta E_{\rm HOMO \rightarrow LUMO}$  was obtained as; (L¹) 3.693 > (L²) 3.654 > (3) 3.085 > (12) 2.967 > (11) 2.926 > (4) 2.912 > (7) 2.847 > (2) 1.728. The molecules having minor frontier orbital band difference are highly chemical reactive as well as more polarizable. The calculated values of  $\Delta E_{\rm HOMO \rightarrow LUMO}$  suggested that the studied complexes have small band gap. Therefore, the complexes were found to be more reactive than the ligands.

It could be observed from figure that for both ligands  $(L^1)$  and  $(L^2)$ , the electron density of HOMO and LUMO is concentrated on the entire structures with the exception of methoxy groups. Likewise, in LUMO of complex (2), the charge density is only accomulated at half part of the complex. Whie in the LUMO of all the other stidied complexes, the charge density is distributed over the entire complex structure. But in the HOMO of complex (2) and (7), the charge density is only focused at central part, mainly at the central metal ions and phenylenediamine-azomethine fragments. Whereas in the HOMO of all the other studied complexes, the charge density is dispersed over the complete complex structure.

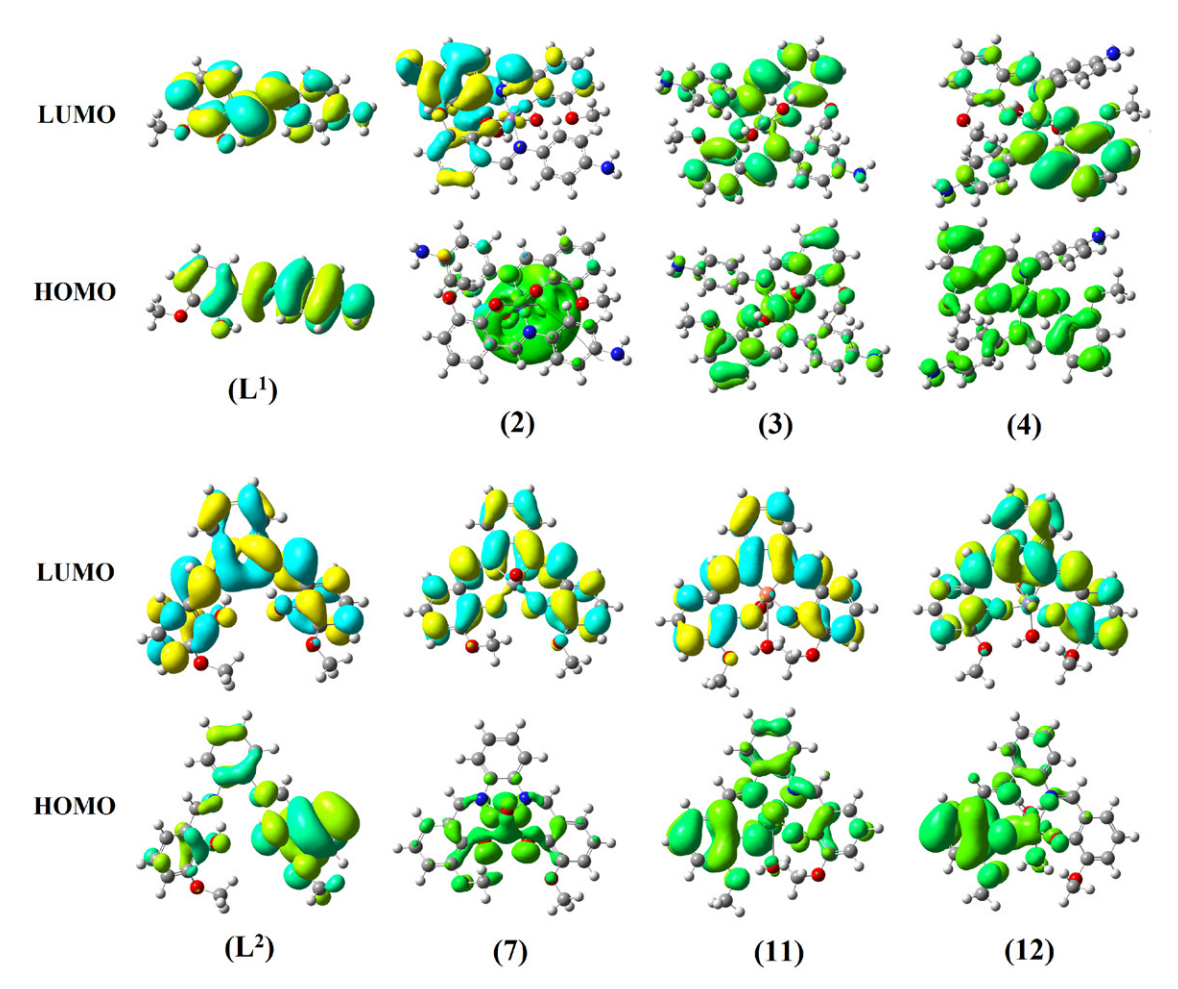


Figure 3. Frontier molecular orbitals (FMOs') illustrating distribution of electronic charge density in ligands and their selected metal complexes

**Table 3.** FMO energies and their energy gaps ( $\Delta E$ ) for phenylenediamine based ligands and their selected metal complexes

D ( W)	Compounds							
Descriptor (eV)	$(L^1)$	$(L^2)$	(2)	(3)	(4)	(7)	(11)	(12)
$E_{LUMO}$	-1.796	-2.232	-1.483	-1.039	-1.484	-2.235	-1.891	-1.860
$E_{HOMO}$	-5.489	-5.886	-3.211	-4.124	-4.396	-5.082	-4.817	-4.827
$\Delta E_{HOMO \rightarrow LUMO}$	3.693	3.654	1.728	3.085	2.912	2.847	2.926	2.967
Ionization Potential (IP)	5.489	5.886	3.211	4.124	4.396	5.082	4.817	4.827
Electron Affinity (EA)	1.796	2.232	1.483	1.039	1.484	2.235	1.891	1.860
Global Hardness (η)	1.847	1.827	0.864	1.543	1.456	1.424	1.463	1.484
Chemical Potential (µ)	-3.643	-4.059	-2.347	-2.582	-2.940	-3.659	-3.354	-3.344
Global Softness (S)	0.271	0.274	0.579	0.324	0.343	0.351	0.342	0.337
Electronegativity (χ)	3.643	4.059	2.347	2.582	2.940	3.659	3.354	3.344
Electrophilicity (ω)	3.593	4.509	3.188	2.160	2.968	4.701	3.845	3.768

### 3. 8. Chemical Reactivity Parameters

The FMO band gap ( $\Delta E$ ) is a remarkable factor to investigate and describe the chemical reactivity parameters such as the accepting and donating ability of the studied molecules along with their hardness and softness.<sup>55</sup> Molecules with a high FMO energy difference are kinetically least reactive and more stable, which makes them chemically hard in nature. While the molecules with small FMO band gaps are kinetically more reactive in nature which makes them chemically soft and less stable with more polarizability. Global reactivity parameters<sup>56</sup> like electron affinity (EA), ionization potential (IP), global softness ( $\sigma$ ), chemical potential ( $\mu$ ), global hardness ( $\eta$ ), global electrophilicity ( $\omega$ ) in addition to electronegativity  $(\chi)$  can be determined using FMO energy gap employing equations S1-S6 and the values are shown in Table 3. Electronegativity is considered as the most important chemical parameter that describes the competency of any chemical system for attracting the electrons. The stability of any molecule is specified by the negative readings of the chem-

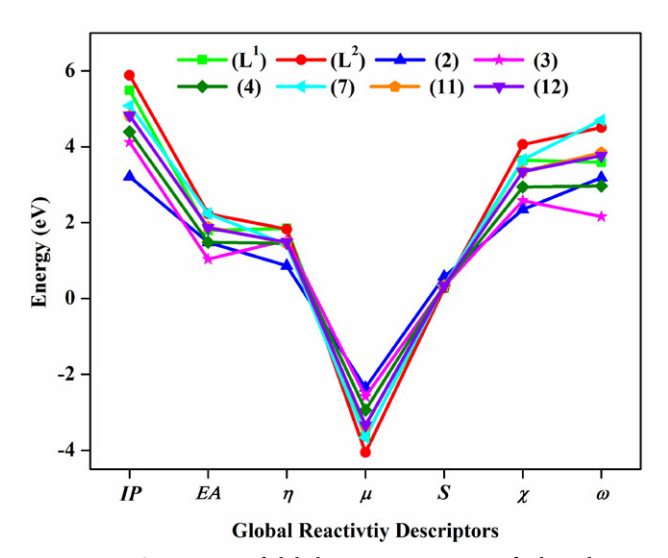


**Figure 4.** Comparison of global reactivity parameters for ligands vs metal complexes

ical potential (µ). This remarkable study could play an imperative impact in the domain of experimental investigation and particularly in the biological assay of chemical systems.<sup>57</sup> It can be witnessed from the table that the ionization potential (5.886 eV) in ligand (L<sup>2</sup>) is more, having most negative chemical potential (-4.059 eV), greater values of electron affinity (2.232 eV) and electronegativity (4.059 eV) than  $(L^1)$ . In addition, there exist a straight link between the FMO energy gap and the hardness, consequently the compound with a more FMO energy difference is the chemically less reactive. As a result, the calculated FMO energy differences and hardness are greater, while softness readings are smaller for (L1) in comparison to  $(L^2)$ , signifying that  $(L^2)$  is more reactive and less stable. The detailed comparison of global reactivity parameters for all the studied compounds is illustrated by Figure 4.

# 3. 9. Molecular Electrostatic Potential (MEP) Analysis

Molecular electrostatic potential (MEP) map is linked to electronic charge density and with the help of it, the chemical reactivity and noncovalent interactions such as nucleophilic and electrophilic attack sites can be comprehend. MEP map is the graphical interpretation of the three dimensional electronic charge. With the help of this 3D map, the physical as well as chemical characteristic features of any chemical structure can also be elucidated.<sup>58</sup> In the MEP map, the charge is distributed around the molecule in space which helps to understand the hydrogen bonding, reactive positions for the attack by electrophiles and nucleophiles as well and biological recognition procedures. It is known as supportive parameter that provides assistance to characterize the zone, size, positive, negative and shape of an investigated chemical structure. The electrostatic potential values are assessed with different shades. The negative region of electrostatic potential is denoted by red colour, while the blue and green colours represent the positive and less positive region of MEP respectively. Different code colours in the terms of potential fallows following order; blue > green > yellow > orange > red.

By using density functional B3LYP/6-311++G(d, p) basis set, MEP is designed over optimized geometrical structures of the studied compounds and the MEP plots are displayed in Figure 5. An analysis of the MEP plots suggested that in the investigated compounds, the red colour (negative region) was localized around Ohvdroxvl and O<sub>methoxy</sub> atoms. Hence, it is an electron rich part and could be potential place for the attack by electrophile. In contrast, the blue colour (positive region) defining the electron deficient area was localized around Namino and Nazomethine atoms together with some of the hydrogen alongside carbon atoms could be a favourable site for the attack by nucleophiles. Whereas, the green zone indicated the average potential, i.e., the part in the middle of two margins. From blue, green and red colours, it was obvious that all these different reaction positions were present in all studied compounds. The studied metal complexes possess electron deficient sites with smaller electronegativity which are the preferred positions for an attack by nucleophilic species. The computed MEP plots were found to be in agreement with the computed atomic charges contained by studied chemical molecules. Thus, signifying that on complexation, the intra-molecular charge dispersal produced an electropositive zone at the central metal atoms that might influence their various physicochemical properties.

#### 3. 10. Natural Bond Orbital (NBO) Analysis

NBO analysis is an effective practice that proficiently interprets the intramolecular interactions and delocalization of electronic charge density. It provides proper details to analyse and explain the intra-molecular hydrogen bonding as well as transfer of electronic charge from the filled orbitals to free orbitals by employing the second-order Fock matrix. By means of equation 1, the stabilization energies of the investigated molecules have been calculated, and some

significant NBO interactions are depicted in Table S2. NBO analysis indicated the existence of resonance/ $\pi$ -conjugation attributable to delocalization of  $\pi$ -electrons in addition to strong intra-molecular primary or secondary hyper-conjugative interactions in the investigated compounds. From the findings attained in valence hybrids of NBO's, the NBO analysis also provides significant perceptions about the polarity of different bonds within the studied molecular systems. The NBO results also signify the involvement of extra valence orbitals in the composition of natural bond orbitals that has notable contribution regarding the stabilization energy within the examined molecules. <sup>59</sup> The NBO analysis is also important as it explains the nature of any definite bond through evaluating the interactions between donating and accepting orbitals.

$$E^{(2)} = q_i \frac{(F_{i,j})^2}{\epsilon_i - \epsilon_j} \tag{1}$$

In this equation,  $E^{(2)}$  defines the stabilization energy,  $q_i$  symbolizes the vacancy of the contributor orbital,  $F_{(i,i)}$ denotes the diagonal while  $\varepsilon_i$  and  $\varepsilon_i$  indicate the off diagonal NBO Fock matrix features. In this NBO study, interactions between electron donating and accepting orbitals are exposed by the stabilization energy  $E^{(2)}$  value. The larger value of stabilization energy E(2) indicates that greater interaction is found between electron acceptors and donors. The overlapping of  $\sigma(C-C)$  with  $\sigma^*(C-C)$  bonding orbitals causes molecular interaction, that is producing the intramolecular charge to stabilize the system. When there is higher electronic charge density in C-C antibonding orbital, these interactions are observed which weakens corresponding bonds.<sup>60</sup> The electron density due to single and double bond of the conjugated ring exhibits strong delocalization within the chemical systems. The interaction energy inferred from second order perturbation theory analysis of Fock Matrix. The analysis was performed for

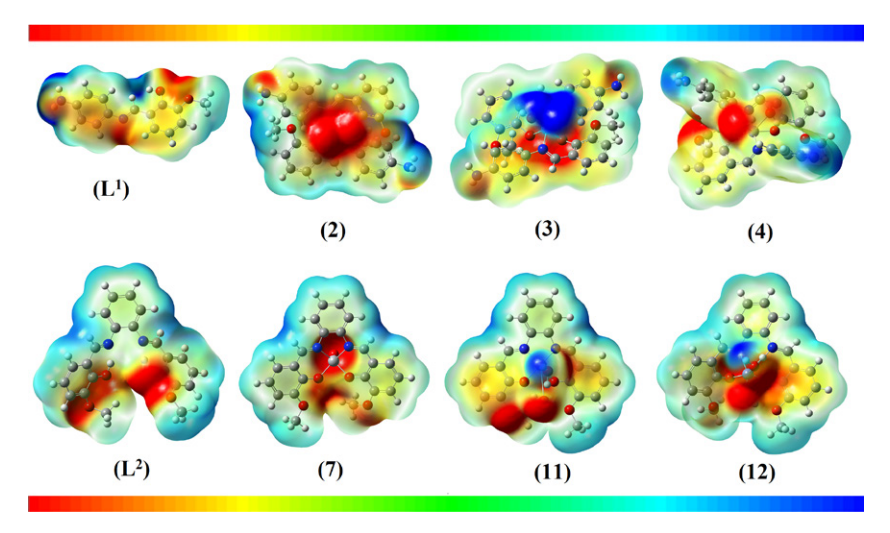


Figure 5. MEPs and colour pattern for the investigated ligands and their selected metal complexes

studied compounds by investigating all the promising interactions regarding occupied Lewis style donors and vacant non Lewis type acceptor, while their status of energies is estimated by second order perturbation theory.

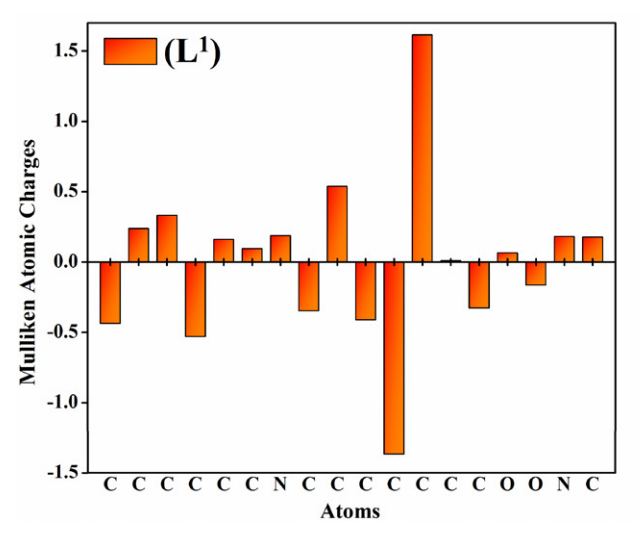
Usually, four major types of electronic transitions including  $\sigma \rightarrow \sigma^*$ , LP $\rightarrow \sigma^*$ ,  $\pi \rightarrow \pi^*$ , along with LP $\rightarrow \pi^*$  are seen for any studied molecule. The observed  $\pi \rightarrow \pi^*$  type of transitions have an additional estimation, while transitions such as LP $\rightarrow \sigma^*$  as well as LP $\rightarrow \pi^*$  demonstrated quite appropriate values for stabilization energy  $E^{(2)}$ . Moreover, the least  $E^{(2)}$  values were shown by  $\sigma \rightarrow \sigma^*$  electronic transitions. The highest readings for  $\pi \rightarrow \pi^*$  transitions were  $\pi(C_2-C_3) \rightarrow \pi^*(C_1-C_6), \quad \pi(C_{21}-C_{22}) \rightarrow \pi^*(N_{14}-C_{24})$  with stabilization energies of 21.46 and 21.54 kcal/mol in ligands (L1) and (L2), correspondingly. Although, some other  $\pi \rightarrow \pi^*$  electronic transitions having significant values of stabilization energy were also observed like  $\pi(C_8 C_{13}$ ) $\rightarrow \pi^*(C_9-C_{10}), \ \pi(C_4-C_5)\rightarrow \pi^*(C_1-C_6), \ \pi(C_{11}-C_{12})\rightarrow$  $\pi^*(N_7-C_{14}), \ \pi(C_9-C_{10}) \rightarrow \pi^*(C_8-C_{13}) \ \text{and} \ \pi(C_1-C_6) \rightarrow \pi^*$  $(C_2-C_3)$  in  $(L^1)$  with 18.68, 18.67, 18.38, 17.77 and 16.25 kcal/mol, whereas  $\pi(C_3-C_4)\rightarrow \pi^*(C_1-C_2)$ ,  $\pi(C_5-C_6)\rightarrow$  $\pi^*(C_1-C_2), \quad \pi(C_7-C_8) \rightarrow \pi^*(C_9-C_{10}), \quad \pi(C_1-C_2) \rightarrow \pi^*(C_3-C_{10})$  $C_4$ ),  $\pi(C_{18}-C_{23}) \rightarrow \pi^*(C_{19}-C_{20})$ ,  $\pi(C_{19}-C_{20}) \rightarrow \pi^*(C_{18}-C_{23})$ and  $\pi(C_9-C_{10}) \rightarrow \pi^*(C_7-C_8)$  in (L<sup>2</sup>) with stabilization energy of 20.54, 20.54, 20.54, 20.09, 18.30, 17.61 and 17.34 kcal/mol, respectively. These electronic transitions strongly stabilize both the ligands  $(L^1)$  and  $(L^2)$ .

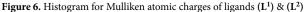
Similar type of interaction linked to resonance in the structure was observed between the oxygen lone pair  $O_{15}$ ,  $O_{12}$  and the anti-periplanar  $C_{11}$ – $C_{12}$ ,  $C_7$ - $C_8$  antibond which gave 27.24 and 65.17 kcal/mol energy of stabilization in ( $\mathbf{L}^1$ ) and ( $\mathbf{L}^1$ ), respectively. It is evident from the NBO analysis that strong interactions, charge transfer properties, stabilization energies, coordination tendency and stability exist in the studied ligands ( $\mathbf{L}^1$ ) and ( $\mathbf{L}^2$ ). Likewise, the foremost  $\pi \rightarrow \pi^*$  interactions including;  $\pi(C_{29}$ – $C_{30}$ ) $\rightarrow \pi^*(N_{24}$ – $C_{31}$ ),  $\pi(C_{29}$ – $C_{30}$ ) $\rightarrow \pi^*(N_{24}$ – $C_{31}$ ),  $\pi(C_{29}$ – $C_{30}$ ) $\rightarrow \pi^*(N_{24}$ – $C_{31}$ ),  $\pi(C_{29}$ – $C_{30}$ ) $\rightarrow \pi^*(N_{24}$ – $C_{31}$ ),  $\pi(C_{29}$ – $C_{30}$ ) $\rightarrow \pi^*(N_{24}$ – $C_{31}$ ),  $\pi(C_{29}$ – $C_{30}$ ) $\rightarrow \pi^*(N_{24}$ – $C_{31}$ ),  $\pi(C_{29}$ – $C_{30}$ ) $\rightarrow \pi^*(N_{24}$ – $C_{31}$ ),  $\pi(C_{29}$ – $C_{30}$ )

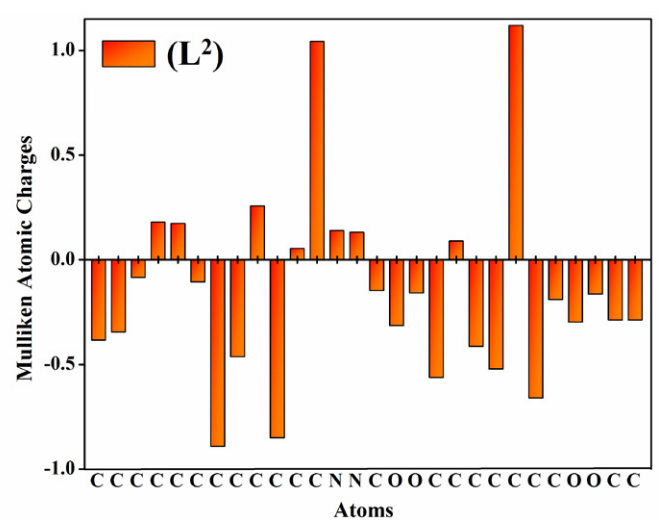
 $C_3) \rightarrow \pi^*(C_4 - C_5)$ ,  $\pi(C_{24} - C_{25}) \rightarrow \pi^*(N_{16} - C_{26})$  and  $\pi(C_{20} - C_{21}) \rightarrow \pi^*(C_{24} - C_{25})$  produced 18.39, 38.68, 10.64, 17.72 and 23.42 kcal/mol stabilization energies for complexes (2), (4), (7), (11) and (12) correspondingly. In addition, the LP $\rightarrow \pi^*$  transitions were observed as;  $C_{10} \rightarrow \pi^*(C_8 - C_9)$ ,  $C_{12} \rightarrow \pi^*(N_7 - C_{14})$ ,  $C_{23} \rightarrow \pi^*(N_{15} - C_{25})$ ,  $C_{22} \rightarrow \pi^*(C_{20} - C_{21})$  and  $C_{14} \rightarrow \pi^*(C_9 - C_{10})$  with higher stabilization energies of 39.85, 125.84, 69.47, 41.41 and 64.55 kcal/mol for complexes (2), (4), (7), (11) and (12) respectively. This NBO analysis showed extended hyperconjugation and notable intramolecular interactions of studied compounds.

# 3. 11. Mulliken Atomic Charge (MAC) Analysis

In chemistry, chemical reactivities, electromagnetic spectra accompanied by NMR chemical shifts, electric potentials and dipole moments are considered as recognizable parameters of molecules which could have direct association with atomic charges in the chemical systems. Various theories regarding the structural features of chemical systems entirely depend on the concept of Mulliken atomic charges. The calculation of atomic charges for the preferred chemical systems by computational chemistry play supportive role to evaluate and explain the experimental data. It is particularly important to deeply comprehend the characterization of atomic charges to understand and describe the applications of any chemical system.<sup>61</sup> The Mulliken atomic charges of investigated compounds were determined by employing B3LYP level and 6-311++G(d, p) basis set. The Mulliken charges are listed in Tables S3 & S4, while their histograms are presented in Figure 6 & 7. The charge dispersion of the studied compounds displayed that the all oxygen and nitrogen atoms in addition to the carbon atoms linked with oxygen and nitrogen atoms were negatively charged. Whereas, greater positive values were found for the other carbon and hydrogen atoms together







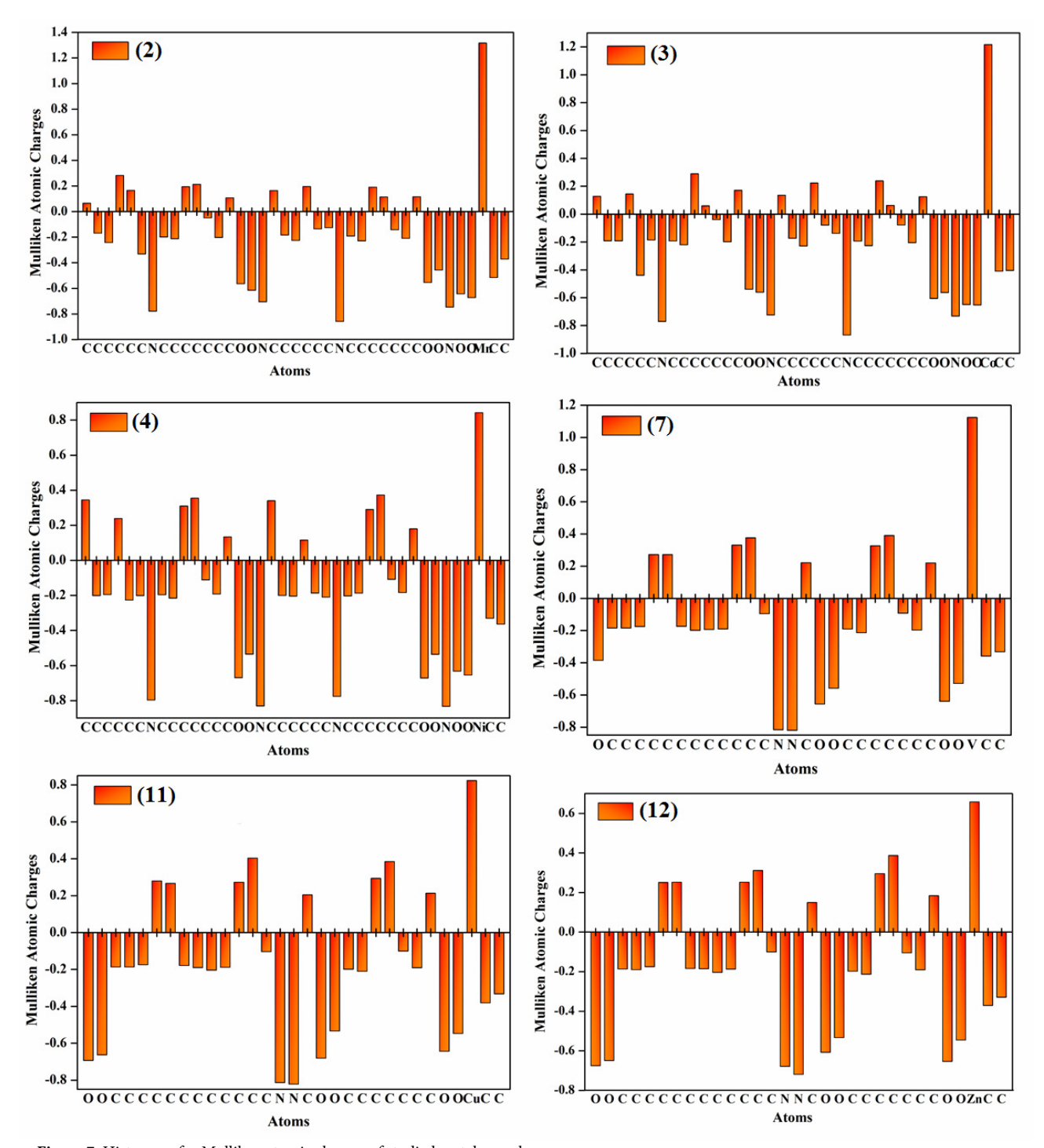


Figure 7. Histogram for Mulliken atomic charges of studied metal complexes

with metals (Mn, Co, Ni, V, Cu and Zn) in the studied metal complex (2), (3), (4), (7), (11) and (12).

#### 3. 12. Computed UV-Vis Analysis

UV-Visible spectroscopy gave valuable explanation on the charge transfer potentials of the investigated compounds. To get the insights concerning the theoretical UV-

Vis spectra of the ligands together with their selected metal complexes, TD-DFT calculation were executed at B3LYP/6-311++G(d, p) level. The transition energy values, maximum absorption wavelength ( $\lambda_{max}$ ), oscillator strength ( $f_{os}$ ) together with minor and major molecular orbital transitions of the studied compounds are tabulated in Table S5. Whereas, the theoretical UV-Vis spectra are shown in Figure S9.

## 3. 13. Computed IR Analysis

The synthesized ligands (L1) and (L2) having 32 and 48 atoms correspondingly comprising carbon, oxygen, hydrogen and nitrogen atoms. The harmonic vibrational frequencies of both ligands were computed using B3LY-P/6-311++G(d, p). Both the ligands contain 90 and 138 vibrational modes correspondingly with singlet spin and point group symmetry C1. The calculated vibrational modes of atoms were assigned using the animation option of Gauss View software. All the vibrational assignments associated with theoretical infrared spectral values were taken into consideration while only the most prominent vibrational frequencies with high accuracy are listed in Tables S6 & S7. Figure 8 illustrates the theoretically simulated scaled infrared spectra of all studied compounds. The theoretical frequencies were found to be greater than the experimentally observed values and the obvious reason would be the overestimation of the computed vibrational modes because of the negligence of anharmonicity in the actual chemical system.

With the aim to reduce the frequency values analogous to that of experimental values, electron correlation would be included in density functional theory. The overall practice is to scale down the computed vibrational frequencies to compare the frequency values obtained after the experiment. The scaling factor approach is very valu-

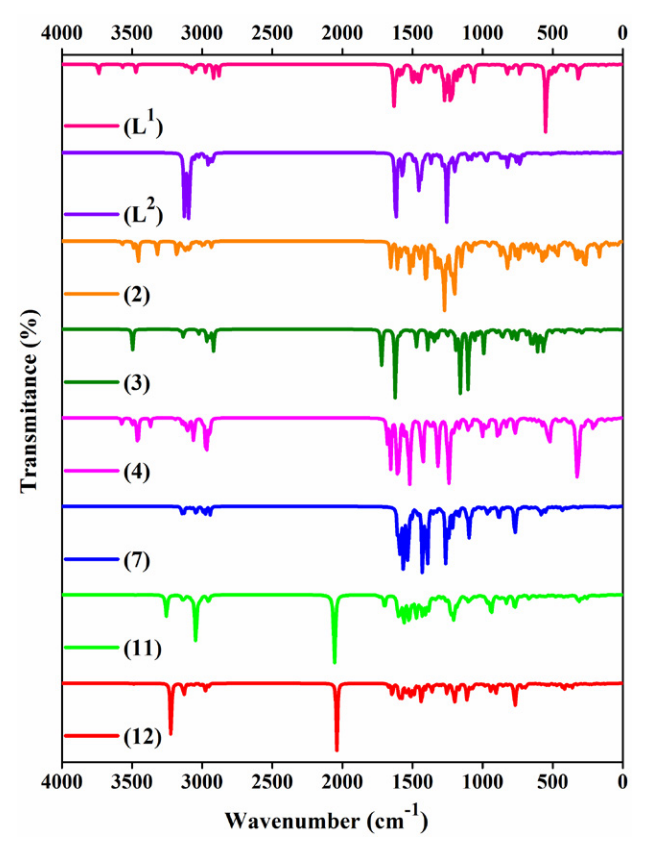


**Figure 8.** Computed IR spectra for phenylenediamine Schiff base ligands and their selected metal complexes

able for correlating the theoretical vibrational frequencies to the practically investigated frequencies. Thus, the scaling factor (0.9742) of B3LYP/6-311++G(d, p) was utilized to precise the systematic defects *i.e.*, to neglect of basis set defects along with some enharmonic effects.<sup>62</sup> Experimental infrared spectra of ligands were compared with the theoretically simulated scaled infrared spectra, followed by comprehensive frequency assignments. The important functional groups are described here in detail:

O-H vibrations: The O-H stretching vibration was found at 3744, 3123 cm<sup>-1</sup> (theoretical) and 3427, 3230 cm<sup>-1</sup> (experimental) for ligand (L<sup>1</sup>) and (L<sup>2</sup>), respectively.

 $\rm NH_2$  vibrations: The vibrational modes for  $\rm NH_2$  were observed at 3478 and 3574 cm<sup>-1</sup> (theoretical) and 3020 cm<sup>-1</sup> (experimental).

HC=N vibration: The HC=N vibrations were detected at 1617, 1619 cm $^{-1}$  (theoretical) and 1640, 1638 cm $^{-1}$  (experimental) for ligand ( $L^1$ ) and ( $L^2$ ), correspondingly.

The DFT-based theoretical vibrational modes have obtained to be consistent with the practically determined findings.

# 3. 14. Antibacterial Activity

The as-synthesized compounds were investigated for in vitro antibacterial activity against three G- bacteria (GNB) i.e., Salmonella typhi, Klebsiella pneumonia, Escherichia coli along with one G+ bacteria (GPB) i.e., Staphylococcus aureus. Two reference drugs i.e., ampicillin (SD<sup>1</sup>) and streptomycin (SD<sup>2</sup>) were used to compare the results of antibacterial activity of investigated compounds (Table 4, Figure 9). The results showed that DMSO had no interference on antibacterial activity of the compounds. Both the uncomplexed ligands exhibited antibacterial activity against all bacteria except (L<sup>2</sup>) that showed no activity against Klebsiella pneumonia. Overall, ligand (L1) exhibited more activity. It showed maximum and minimum activity against Staphylococcus aureus and Klebsiella pneumonia with 17 and 05 mm zones of inhibition, respectively. While (L2) exhibited highest activity against Escherichia coli with 18 mm zone of inhibition.

All the complexes exhibited significant antibacterial activity against all bacteria except complexes (2) and (4) that were inactive against *Klebsiella pneumonia* and *Staphylococcus aureus*, correspondingly. Among all the complexes, the zinc complexes were found to be the most active. The complexes (12) and (6) displayed the maximum activity of 29 and 28 mm against *Staphylococcus aureus*. While both complexes (12) and (6) exhibited moderate inhibitory activity of 23 mm against *Escherichia coli*, correspondingly. The complex (3) inhibited 23, 22, 21 and 16 mm zones of *Klebsiella pneumonia*, *Salmonella typhi*, *Escherichia coli* and *Staphylococcus aureus*, respectively. The complexes (7) and (8) demonstrated least antibacterial profile with 6 and 7 mm inhibition zones against *Staphylococcus aureus* and *Salmonella typhi*, correspondingly.

Table 4. Antibacterial activity (inhibition zone/mm) of ligands and their metal complexes

Compounds	Salmonella typhi (G-)	Klebsiella pneumonia (G-)	Escherichia coli (G-)	Staphylococcus aureus (G+)	
(L <sup>1</sup> )	15	05	15	17	
$(L^2)$	17	0	18	16	
(1)	14	22	06	19	
(2)	21	23	11	0	
(3)	22	23	16	21	
(4)	21	0	21	0	
(5)	19	15	17	20	
(6)	20	23	19	28	
(7)	14	20	05	06	
(8)	07	16	23	23	
(9)	21	09	07	09	
(10)	18	21	22	19	
(11)	22	18	15	20	
(12)	19	22	23	29	
$(SD^1)$	29	38	35	30	
$(SD^2)$	35	39	37	40	

SD1 = Ampicillin, SD2 = Streptomycin

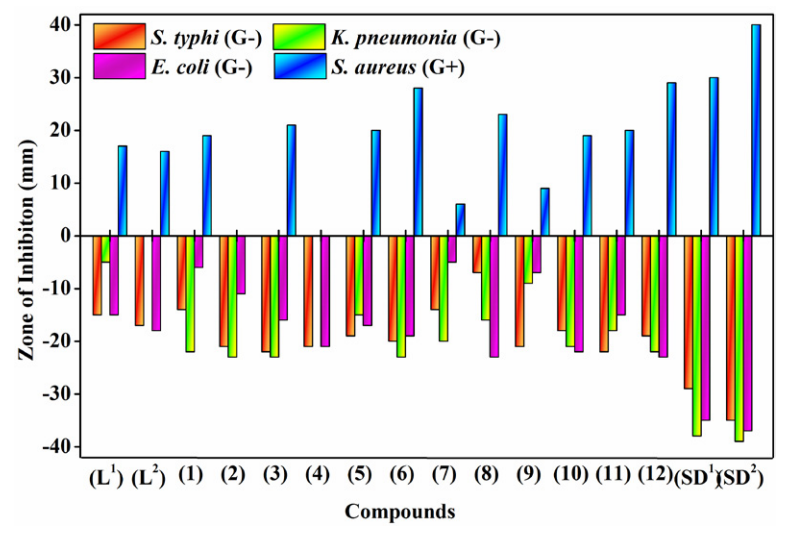


Figure 9. Antibacterial activity of phenylenediamine Schiff base derived compounds against Gram-positive and Gram-negative bacteria

#### 4. Conclusion

In the current situation of increasing global drug resistance coupled with the scarcity of efficient antibacterial drugs, two new symmetrical ligands ( $L^1$ )–( $L^2$ ) and their derived metal chelates were synthesized and experimentally characterized through physical, elemental, spectral data along with computational study by DFT/B3LY-P/6-311++G(d,p) approach. The spectral assignments of all the metal based phenylenediamine compounds confirmed that the deprotonated bidentate and tetradentate Schiff base ligands bonded with 3d-metal cations through phenolic oxygen and azomethine nitrogen along with two water molecules resulting in the formation of a stable six-membered chelate ring. Based on the magnetic mo-

ments and electronic spectra, an octahedral geometry was recommended for all the divalent metal complexes except for tetravalent vanadyl complexes that exhibited square pyramidal geometry, thus correlating accurately with the assessed molecular formula. On the basis of molar conductivity, all the metal complexes formed were declared as neutral having no free anions outside the coordination sphere. The theoretically obtained structural features accorded effectively with experimentally determined structural findings. This reasonable constancy validated that the chosen DFT method might be a realistic approach to comprehend some other characteristic features of the studied compounds. The charge transfer properties, kinetic stability and chemical reactivity of the studied compounds were evaluated by FMO analysis. Antibacterial activity of all the

phenylenediamine derived compounds was evaluated. The results of bioactivity concluded that both the phenylenediamine ligands have shown significant antibacterial potential which was further intensified upon chelation owing to the transference of charge from metal to ligand. Overall, the Zn(II) complex possessed higher antibacterial activity. The results conclude that these metal based compounds have the aptitude to be converted into drug candidates and this study will be valuable to design and develop promising metal-based drugs to treat microbial infections.

#### Acknowledgements

The authors are grateful to the Higher Education Commission (HEC) of Pakistan for providing financial assistance through the NRPU Project # 7800.

#### Conflict of Interest

All authors declared that they have no conflict of interest.

## 5. References

- W. Zafar, S. H. Sumrra, Z. H. Chohan, Eur. J. Med. Chem. 2021, 222, 113602.
  - DOI:10.1016/j.ejmech.2021.113602
- H. Kargar, R. Behjatmanesh-Ardakani, V. Torabi, M. Kashani,
   Z. Chavoshpour-Natanzi, Z. Kazemi, V. Mirkhani, A. Sahraei,
   M. N. Tahir, M. Ashfaq, K. S. Munawar, *Polyhedron*, 2021,
   195, 114988. DOI:10.1016/j.poly.2020.114988
- S. A. Beyramabadi, M. Saadat-Far, A. Faraji-Shovey, M. Javan-Khoshkholgh, A. Morsali, J. Mol. Struct. 2020, 1208, 127898. DOI:10.1016/j.molstruc.2020.127898
- H. Kargar, V. Torabi, A. Akbari, R. Behjatmanesh-Ardakani,
   M. N. Tahir, *J. Mol. Struct.* 2019, 1179, 732–738.
   DOI:10.1016/j.molstruc.2018.11.066
- A. Sahraei, H. Kargar, M. Hakimi, M. N. Tahir, J. Mol. Struct.
   2017, 1149, 576–584. DOI:10.1016/j.molstruc.2017.08.022
- P. Sen, T. Nyokong, *Polyhedron*, **2019**, *173*, 114135.
   DOI:10.1016/j.poly.2019.114135
- S. H. Sumrra, Z. Arshad, W. Zafar, K. Mahmood, M. Ashfaq,
   A. U. Hassan, E. U. Mughal, A. Irfan, M. Imran, R. Soc. Open Sci. 2021, 8, 210910. DOI:10.1098/rsos.210910
- 8. H. Kargar, A. A. Ardakani, M. N. Tahir, M. Ashfaq, K. S. Munawar, *J. Mol. Struct.* **2021**, *1233*, 130112.
  - **DOI:**10.1016/j.molstruc.2021.130112
- X. H. Qi, Z. M. Wu, S. B. Wang, B. X. Wang, L. L. Wang, H. Li,
   Q. Guo, J. Coord. Chem. 2019, 14, 2310–2325.
   DOI:10.1080/00958972.2019.1647535
- S. H. Sumrra, U. Habiba, W. Zafar, M. Imran, Z. H. Chohan, J. Coord. Chem. 2020, 73, 2838–2877.
   DOI:10.1080/00958972.2020.1839751
- 11. Y. J. Ren, J. L. Zhu, L. X. Zhang, Y. X. Xu, S. S. Qian, *Acta Chim. Slov.* 2017, 64, 825–831. **DOI:**10.17344/acsi.2017.3315

- S. Yasmeen, S. H. Sumrra, M. S. Akram, Z. H. Chohan, J. Enzyme Inhib. Med. Chem. 2017, 32, 106–112.
   DOI:10.1080/14756366.2016.1238363
- K. Buldurun, N. Turan, E. Bursal, A. Mantarcı, F. Turkan, P. Taslimi, İ. Gülçin, *Res. Chem.* Intermed. 2020, 46, 283–297.
   DOI:10.1007/s11164-019-03949-3
- M. Kumbar, S. A. Patil, S. S. Toragalmath, S. S. Jawoor, A. Shettar, *Inorg. Chim. Acta.* **2020**, *500*, 119210.
   **DOI:**10.1016/j.ica.2019.119210
- X. S. Cui, J. Chen, K. Y. Chai, J. S. Lee, Z. S. Quan, Med. Chem. Res. 2009, 18, 49–58.
  - DOI:10.1007/s00044-008-9106-3
- S. S. Hassan, S. M. Gomha, Chem. Pap. 2018, 73, 331–344.
   DOI:10.1007/s11696-018-0592-6
- D. Śmiłowicz, N. Metzler-Nolte, J. Inorg. Biochem. 2020, 206, 111041. DOI:10.1016/j.jinorgbio.2020.111041
- H. Kargar, F. Aghaei-Meybodi, R. Behjatmanesh-Ardakani, M. R. Elahifard, V. Torabi, M. Fallah-Mehrjardi, M. N. Tahird, M. Ashfaq, K. S. Munawar, J. Mol. Struct. 2021, 1230, 129908. DOI:10.1016/j.molstruc.2021.129908
- S. H. Sumrra, W. Zafar, H. Javed, M. Zafar, M. Z. Hussain, M. Imran, M. A. Nadeem, *BioMetals*, 2021, 1-23.
   DOI:10.1007/s10534-021-00345-6
- Z. D. Petrović, J. Đorović, D. Simijonović, S. Trifunović, V. P. Petrović, *Chem. Pap.* 2018, 72, 2171–2180.
   DOI:10.1007/s11696-018-0419-5
- Z. Shokohi-Pour, H. Chiniforoshan, M. R. Sabzalian, S. A. Esmaeili, A. A. Momtazi-borojeni, *J. Biomol. Struct. Dyn.* 2018, 36, 532–549. DOI:10.1080/07391102.2017.1287006
- A. Jamshidvand, M. Sahihi, V. Mirkhani, M. Moghadam, I. Mohammadpoor-Baltork, S. Tangestaninejad, H. A. Rudbari, H. Kargar, R. Keshavarzi, S. Gharaghanic, *J. Mol. Liq.* 2018, 253, 61–71. DOI:10.1016/j.molliq.2018.01.029
- Jarrahpour, D. Khalili, E. D. Clercq, C. Salmi, J. M. Brunel, *Molecules*, 2007, 12, 1720–1730. **DOI:**10.3390/12081720
- S. N. Shukla, P. Gaur, M. L. Raidas, B. Chaurasia, *J. Mol. Struct.* 2020, 1202, 127362. DOI:10.1016/j.molstruc.2019.127362
- A. A. Abdel-Aziz, S. H. Seda, J. Fluoresc. 2017, 27, 1051–1066.
   DOI:10.1007/s10895-017-2039-9
- S. S. Wu, W. B. Yuan, H. Y. Wang, Q. Zhang, M. Liu, K. B. Yu, J. Inorg. Biochem. 2008, 102, 2026–2034.
   DOI:10.1016/j.jinorgbio.2008.08.005
- S. Khalid, S. H. Sumrra, Z. H. Chohan, Sains Malays. 2020, 49, 1891–1904. DOI:10.17576/jsm-2020-4908-11
- 28. Z. H. Chohan, S. H. Sumrra, *Appl. Organomet. Chem.* 2010, 24, 122–130. **DOI:**10.1002/aoc.1590
- 29. M. J. Frisch et al. (2009) Gaussian 09, Revision D.01; Gaussian, Inc.: Wallingford, CT.
- N. Prabavathi, A. Nilufer, V. Krishnakumar, Spectrochim. Acta A Mol. Biomol. Spectrosc. 2013, 114, 449–474.
   DOI:10.1016/j.saa.2013.05.011
- 31. R. Dennington, T. Keith, J. Millam (2009) Gauss View, Version 5; Semichem, Inc.: Shawnee Mission, KS.
- 32. N. M. O'boyle, A. L. Tenderholt, K. M. Langner, *J. Comput. Chem.* **2008**, *29*, 839–845. **DOI**:10.1002/jcc.20823

- M. D. Hanwell, D. E. Curtis, D. C. Lonie, T. Vandermeersch,
   E. Zurek, G. R. Hutchison, *J. Cheminform.* 2012, 4, 1–17.
   DOI:10.1186/1758-2946-4-17
- 34. G. A. Andrienko, (2010) Chemcraft. Graphical Software for Visualization of Quantum Chemistry Computations.
- A. Sahraei, H. Kargar, M. Hakimi, M. N. Tahir, Transit. Met. Chem. 2017, 42, 483–489. DOI:10.1007/s11243-017-0152-x
- P. Gull, A.A. Hashmi, *J. Mol. Struct.* 2017, 1139, 264–268.
   DOI:10.1016/j.molstruc.2017.03.053
- M. Hanif, Z. H. Chohan, Spectrochim. Acta A Mol. Biomol. Spectrosc. 2013, 104, 468–476. DOI:10.1016/j.saa.2012.08.026
- G. Ramesh, S. Daravath, N. Ganji, A. Rambabu, K. Venkateswarlu, *J. Mol. Struct.* 2020, 1202, 127338.
   DOI:10.1016/j.molstruc.2019.127338
- M. A. Diab, G. G. Mohamed, W. H. Mahmoud, A. Z. El-Sonbati, S. M. Morgan, S. Y. Abbas, *Appl. Organomet. Chem.* 2019, 33, e4945. DOI:10.1002/aoc.4945
- M. R. Hasan, M. A. Hossain, M. A. Salam, M. N. Uddin, *J. Taibah* Univ. Sci. 2016, 10, 766–773.
   DOI:10.1016/j.jtusci.2015.11.007
- A. U. Hassan, S. H. Sumrra, M. N. Zafar, M. F. Nazar, E. U. Mughal, M. N. Zafar, M. Iqbal, *Mol. Divers.* 2021, 1–22.
   DOI:10.1007/s11030-020-10157-4
- H. Kargar, Transit. Met. Chem. 2014, 39, 811–817.
   DOI:10.1007/s11243-014-9863-4
- R. C. Maurya, D. Sutradhar, M. H. Martin, S. Roy, J. Chourasia, A. K. Sharma, P. Vishwakarma, *Arab. J. Chem.* 2015, 8, 78–92. DOI:10.1016/j.arabjc.2011.01.009
- A. A. Abou-Hussein, W. Linert, Spectrochim. Acta A Mol. Biomol. Spectrosc. 2014, 117, 763–771.
   DOI:10.1016/j.saa.2013.06.078
- 45. G. G. Mohamed, M. A. Zayed, S. M. Abdallah, *J. Mol. Struct.* **2010**, *979*, 62–71. **DOI**:10.1016/j.molstruc.2010.06.002
- M. S. Nair, D. Arish, R. S. Joseyphus, J. Saudi Chem. Soc. 2012, 16, 83–88. DOI:10.1016/j.jscs.2010.11.002
- 47. Y. Xu, L. Xue, Z. G. Wang. Russ, J. Coord. Chem. 2017, 43, 314–319. DOI:10.1134/S1070328417050098
- T. Sedaghat, M. Yousefi, G. Bruno, H. A. Rudbari, H. Motamedi, V. Nobakht, *Polyhedron*, **2014**, *79*, 88–96.
   **DOI:**10.1016/j.poly.2014.04.061

- 49. N. H. Al-Shaalan, *Molecules*, 2011, *16*, 8629-8645. **DOI:**10.3390/molecules16108629
- E. Pahonţu, M. Proks, S. Shova, G. Lupaşcu, D. C. Ilieş, Ş. F. Bărbuceanu, L. Socea, M. Badea, V. Păunescu, D. Istrati, A. Gulea, D. Drăgănescu, C. E. D. Pîrvu, Appl. Organomet. Chem. 2019, 33, e5185. DOI:10.1002/aoc.5185
- O. A. Dar, S. A. Lone, M. A. Malik, M. Y. Wani, M. I. A. Talukdar, A. S. Al-Bogami, A. A. Hashmi, A. Ahmad, *Appl. Orga*nomet. Chem. 2019, 33, e5128.
  - **DOI:** doi.org/10.1002/aoc.5128
- G. P. Dharsini, C. Thanaraj, R. Velladurai, J. Inorg. Organomet. Polym. Mater. 2020, 30, 2315.
   DOI:10.1007/s10904-019-01413-8
- Z. H. Chohan, M. Hanif, Appl. Organomet. Chem. 2011, 25, 753–760. DOI:10.1002/aoc.1833
- R. C. Maurya, B. A. Malik, J. M. Mir, P. K. Vishwakarma, D. K. Rajak, N. Jain, *J. Coord. Chem.* 2015, 68, 2902–2922.
   DOI:10.1080/00958972.2015.1064526
- I. Seghir, N. Nebbache, Y. Meftah, S. E. Hachani, S. Maou, *Acta Chim. Slov.* 2019, 66, 629–637.
   DOI:10.17344/acsi.2019.5044
- A. R. Simović, R. Masnikosa, I. Bratsos, E. Alessio, *Coord. Chem. Rev.* 2019, 398, 113011.
   DOI:10.1016/j.ccr.2019.07.008
- K. A. Moltved, K. P. Kepp, J. Phys. Chem. C. 2019, 123, 18432– 18444. DOI:10.1021/acs.jpcc.9b04317
- S. Guidara, H. Feki, Y. Abid, Spectrochim. Acta A Mol. Biomol. Spectrosc. 2014, 133, 856–866.
   DOI:10.1016/j.saa.2014.06.021
- R. P. Gangadharana, S.S. Krishnan, *Acta. Phys. Pol. A.* 2014, 125, 18–22. DOI:10.12693/APhysPolA.125.18
- A. S. G. El-hak, A. A. Mohammed, A. F. A. Hakiem, R. M. Mahfouz, Spectrochim. Acta A Mol. Biomol. Spectrosc. 2019, 222, 117200. DOI:10.1016/j.saa.2019.117200
- A. S. Athmani, F. Madi, I. Laafifi, M. Cheriet, N. Issaoui, L. Nouar, R. Merdes, *J. Struct. Chem.* 2019, 60, 1906–1916.
   DOI:10.1134/S0022476619120060
- V. S. Kumar, Y. S. Mary, K. Pradhan, D. Brahman, Y. S. Mary,
   R. Thomas, M. S. Roxy, C. V. Alsenoy, *J. Mol. Struct.* 2020,
   1199, 127035. DOI:10.1016/j.molstruc.2019.127035

#### Povzetek

Zanimanje za razvoj naprednih spojin na osnovi kovin, ki zavirajo in kontrolirajo bakterijske okužbe, neprestano narašča. Sintetizirali smo dve novi bioaktivni simetrični mono- in bis- Schiffovi bazi na osnovi fenilendiamina, 2-{[(4-aminofenil) imino]metil}-6-metoksifenol (L¹) in 2,2′-{benzen-1,2-diilbis[nitrilometililiden]}bis(6-metoksifenol) (L²). Spojini smo karakterizirali s fizikalnimi metodami, spektroskopijo, elementno analizo in DFT računalniško analizo z metodo B3LY-P/6-311++G(d, p). Sintetizirali smo koordinacijske spojine obeh novih ligandov z VO, Mn, Co, Ni, Cu in Zn v množinskih razmerjih [M:L, 1:2 in 1:1]. Vse tako pripravljene koordinacijske spojine imajo dobro antibakterijsko delovanje, z najboljšim delovanjem v primeru cinkovih kompleksov. Rezultati kažejo, da so tovrstne spojine obetavne za medicinske aplikacije.



Except when otherwise noted, articles in this journal are published under the terms and conditions of the Creative Commons Attribution 4.0 International License